Geophysical Prospecting, 2006, **54,** 505–514

Wavefield Migration plus Monte Carlo Imaging of 3D Prestack Seismic Data

Ernesto Bonomi,[1]* Leesa M. Brieger,[2] Luca Cazzola[3]** and Francesco Zanoletti[3]

[1]*Environmental and Imaging Sciences Group, CRS4, C.P. 25, I-09010 Pula (CA), Italy,* [2]*present address: San Diego Supercomputer Center, UCSD, 9500 Gilman Dr., La Jolla, CA 92093, USA and* [3]*ENI E&P Division, via Emilia 1, I-20097 San Donato Milanese, Italy*

Received July 2002, revision accepted February 2006

ABSTRACT

Prestack wave-equation migration has proved to be a very accurate shot-by-shot imaging tool. However, 3D imaging with this technique of a large field acquisition, especially one with hundreds of thousands of shots, is prohibitively costly. Simply adapting the technique to migrate many superposed shot-gathers simultaneously would render 3D wavefield prestack migration cost-effective but it introduces uncontrolled non-physical interference among the shot-gathers, making the final image useless. However, it has been observed that multishot signal interference can be kept under some control by averaging over many such images, if each multishot migration is modified by a random phase encoding of the frequency spectra of the seismic traces.

In this article, we analyse this technique, giving a theoretical basis for its observed behaviour: that the error of the image produced by averaging over M phase encoded migrations decreases as M^{-1}. Furthermore, we expand the technique and define a general class of Monte-Carlo encoding methods for which the noise variance of the average imaging condition decreases as M^{-1}; these methods thus all converge asymptotically to the correct reflectivity map, without generating prohibitive costs.

The theoretical asymptotic behaviour is illustrated for three such methods on a 2D test case. Numerical verification in 3D is then presented for one such method implemented with a 3D PSPI extrapolation kernel for two test cases: the SEG–EAGE salt model and a real test constructed from field data.

INTRODUCTION

Echo-reconstruction techniques for subsurface imaging are based on experiments in which short acoustic impulses, emitted at the surface, illuminate a certain volume and are backscattered by inhomogeneities of the medium. Depth migration of prestacked seismic data, which is a central step in the processing flow for hydrocarbon prospecting, is a wave-equation-based process that transforms recorded echoes into acoustic images of the subsurface.

Any migration technique begins with an *a priori* estimate of the velocity field, i.e. a model of the earth's subsurface representing an estimate of the actual propagation velocities. Subsequent iterations of the imaging process are required to improve the initial earth model by perturbing velocities in an effort to obtain optimal focusing of seismic events on their correct depth location (Yilmaz 1987).

In the context of 3D industrial applications, the numerical process involved is a heavy computational task even with modern high-performance computers, demanding much in terms of data storage, data movement and computational effort on parallel architectures (Ober *et al.* 1997; Brieger 2000).

Prestack depth-migration algorithms are usually divided into two classes (Gray *et al.* 2001): wavefield extrapolation techniques, based on the implementation of some form of scalar one-way equation, and Kirchhoff techniques, using ray tracing as the wave propagation model.

*E-mail: *ernesto@crs4.it
**luca.cazzola@eni.it

Wavefield extrapolation techniques are well adapted to common-shot seismic data. In this domain, they naturally split into two independent identical propagation problems, one related to the source wavefield and the other to the recorded wavefield, followed by the standard imaging condition. A suitable choice for the extrapolation is a depth propagation method based on the approximate solution of the one-way equation, either in the (x, y, ω)-domain (Hale 1991; Collino and Joly 1995) or in the (k_x, k_y, ω)-domain (Gazdag and Sguazzero 1984). Common-shot wave-equation migration has proved to be a very accurate imaging tool. Unfortunately, the cost of prestack 3D wavefield extrapolation performed shot by shot, especially with hundreds of thousands of shots, is still prohibitive for industrial data-set applications.

Kirchhoff techniques (Bleistein *et al.* 2001), based on the eikonal approximation of the wave equation associated with the source and receiver locations, are recognized as the most flexible method of imaging prestack seismic data and are useful, regardless of the acquisition geometry. However, Kirchhoff migration using first-arrival traveltime solutions of the eikonal equation, which has been the workhorse reconstruction method for the last decade, may encounter severe imaging inaccuracies in geological situations with fast lateral velocity variations. The use of a more complete description of eikonal propagation, including multipathing, would increase the quality of Kirchhoff-migrated images at the cost of expensive and cumbersome ray-tracing algorithms, which break down near caustics. Although impressive results on multi-arrival Kirchhoff migration or Gaussian-beam migration have been reported (Hill 2001; Xu *et al.* 2001; Notfors *et al.* 2003), their implementation in a production environment remains problematic.

For these reasons and for accuracy of a prestack migration package, we believe that wave-equation prestack migration, although reputed to be computationally more expensive than the Kirchhoff approach, should be used when severe multipathing is present in complex geological situations (Ehinger *et al.* 1996).

A technique allowing the simultaneous wavefield depth extrapolation of many shot-gathers within a single data migration is now well understood and developed. The first proposed method, described by Morton and Ober (1998) and Romero *et al.* (2000), is based on repeated extrapolation of seismic data volumes obtained by the superposition of sources and shot-gathers, where at each iteration the phase of seismic signals is randomly shifted.

As pointed out by Bonomi and Cazzola (1999), a simple analysis shows that the random encoding of the seismic signals leads to a Monte-Carlo quadrature: the resulting imaging condition, averaged over many runs, provides, in addition to the expected correct contribution, spurious random terms that vanish in the limit of a large number of depth migrations. In fact, this is the case when, for each run, the frequency spectra of sources and shot-gathers are encoded with a new sequence of complex random numbers, all independently drawn from the same probability distribution function with a mean value of zero and variance of one. Depending on the distribution, the generalized encoding may shift the *phase* and/or multiply the *amplitude* of each component of the frequency spectra by a random factor. All these concepts have been numerically validated on the SEG–EAGE salt model and on field data, running a prestack migration code which implements a 3D phase-shift-plus-interpolation (PSPI) extrapolation kernel.

We conclude from this work that, for large industrial applications involving hundreds of thousands of shots, in order to achieve an acceptable level of noise, the number of runs need not exceed a small fraction of the number of shots.

PRESTACK WAVE-EQUATION MIGRATION

In this work, the earth's crust is modelled as a three-dimensional half-space: the x- and y-axes are horizontal and the z-axis is vertical, pointing downwards. The model is kept simple with a flat surface and constant density throughout the medium. Pressure waves are assumed to be travelling at point $\mathbf{r} = (x, y, z) = (\mathbf{x}, z)$ with velocity $c(\mathbf{r})$. Let $P(\mathbf{r}_s, \mathbf{r}_g, t)$ denote the pressure measured at time t by a receiver at position $\mathbf{r}_g = (\mathbf{x}_g, z_g)$ after an impulse has been emitted from source position $\mathbf{r}_s = (\mathbf{x}_s, z_s)$ at $t = 0$. For a given shot, the pressure field recorded at each point $\mathbf{r}_g$ is a solution of the scalar wave equation (Stolt 1978).

Migration is an inversion process which reconstructs the map $R(\mathbf{r})$ of local reflectivity from the only available information, i.e. the prestacked volume of seismic data, given by

$$Q(\mathbf{x}_s, \mathbf{x}_g, t) = P(\mathbf{x}_s, 0, \mathbf{x}_g, 0, t) \tag{1}$$

and the velocity field $c(\mathbf{r})$. Reflectors along points of discontinuity in the medium are conceptually located by moving the source and receiver downwards along down- and upgoing wavefronts (Stolt and Benson 1986). As the source and receiver approach each other, the traveltime t approaches zero. At these points, $\mathbf{r} = \mathbf{r}_s = \mathbf{r}_g$, the reflection coefficient R and the wavefield P are related as follows:

$$R(\mathbf{r}) = P(\mathbf{r}, \mathbf{r}, 0). \tag{2}$$

Thus the prestacked migrated seismic volume $P(\mathbf{r}, \mathbf{r}, 0)$ represents, through (2), an image of the subsurface.

To construct the migrated seismic volume, we start from the depth extrapolating formula derived in Appendix A, written in the space–frequency domain as a double convolution,

$$\hat{p}\left(\mathbf{x}_s, \mathbf{x}_g, z+\Delta z, \omega\right) = \sum_{\mathbf{x}'_s, \mathbf{x}'_g} W_{\Delta z}\left(\mathbf{x}_s - \mathbf{x}'_s, \frac{\omega}{c_s}\right) \times W_{\Delta z}\left(\mathbf{x}_g - \mathbf{x}'_g, \frac{\omega}{c_g}\right) \times \hat{p}\left(\mathbf{x}'_s, \mathbf{x}'_g, z, \omega\right), \tag{3}$$

where $\hat{p}(\mathbf{x}_s, \mathbf{x}_g, z, \omega) = \hat{P}(\mathbf{x}_s, z, \mathbf{x}_g, z, \omega)$. To initiate the data extrapolation process, (3) requires the surface initial condition, $\hat{p}(\mathbf{x}_s, \mathbf{x}_g, 0, \omega) = \hat{Q}(\mathbf{x}_s, \mathbf{x}_g, \omega)$. It can be seen that the extrapolator $\hat{W}_{\Delta z}$ is split into two parts, one operating on the source position and the other on the receiver position, with velocities $c_s = c_z(\mathbf{x}'_s)$ and $c_g = c_z(\mathbf{x}'_g)$, respectively.

The methodology, described in Appendix B, to derive an imaging condition for one shot can be generalized to a sequence of N independent shots, for which the resulting prestacked seismic section is written as

$$Q(\mathbf{x}_s, \mathbf{x}_g, t) = \sum_{n=1}^{N} \delta(\mathbf{x}_s - \mathbf{s}_n) Tr^{(n)}(\mathbf{x}_g, t), \tag{4}$$

where $\mathbf{s}_n$ is the source position at the nth shot and $Tr^{(n)}$ represents the resulting field of recorded traces. Using (4) as the initial condition of the iterative extrapolation process defined by (3), we conclude that each common-shot-gather can be migrated independently. The only coupling among the migrated fields is introduced through the imaging condition (A6), which can now be written as

$$R(\mathbf{x}, j\Delta z) = \sum_{n=1}^{N} R^{(n)}(\mathbf{x}, j\Delta z), \qquad j = 1, 2, \ldots. \tag{5}$$

$R^{(n)}$ represents the local reflectivity, calculated using (B6), showing the acoustic image of the earth's crust resulting from the depth extrapolation of the nth shot-gather:

$$R^{(n)}(\mathbf{x}, j\Delta z) = \sum_{\omega} \hat{p}_s^{(n)}(\mathbf{x}, j\Delta z, \omega)\, \hat{p}_g^{(n)}(\mathbf{x}, j\Delta z, \omega). \tag{6}$$

These equations, from which the total image of the subsurface structure can be computed, define in the field coordinate system the canonical imaging condition for seismic data recorded by firing a sequence of N independent shots. Considering that, in marine surveys, N is of the order of hundreds of thousands, equations (5) and (6) illustrate the high computational cost of the prestack processing, thus motivating the development of an adequate compression technique to condense groups of shot-gathers into a unique data set and form an image.

DATA COMPRESSION

In complex geological structures, the illumination induced by a single shot is largely concentrated around normal ray trajectories of the wavefront. In the extrapolation process of a single shot-gather, this simple fact typically results in a proliferation of 'zeros' swamping the partial image of the subsurface (Ehinger *et al.* 1996), thus leading to an enormous loss of computational efficiency when implementing (6).

To avoid a large number of extra calculations, a viable implementation of (5) relies on the decomposition of the velocity model $v(\mathbf{r})$ into subdomains, each one assigned to one shot-gather. However, this approach is potentially a source of difficulties: strongly echoing reflectors, lying outside the subdomain in question but with events present in the shot-gather, will be not correctly migrated and, as a consequence, unwanted artefacts will appear at the boundaries of the resulting partial image. The search for the optimal size of each subdomain, hopefully providing a trade-off between accuracy and efficiency, will be cumbersome in critical geological situations.

To reduce the processing load, another prestack migration strategy can be envisaged by compressing many shot-gathers into a unique data set which covers the entire acquisition domain. A possible strategy may be to superpose linearly all sources into a unique source term and all shot-gathers into a unique gather of traces. The resulting compressed prestacked seismic section can be written as

$$Q^{(N)}(\mathbf{x}_s, \mathbf{x}_g, t) = \sum_{n=1}^{N} \delta(\mathbf{x}_s - \mathbf{s}_n) \sum_{n'=1}^{N} Tr^{(n')}(\mathbf{x}_g, t). \tag{7}$$

Using (7) as the new initial condition for the iterative depth extrapolation formula (3), it follows from the definition of imaging condition (A6) that the map of the local reflectivity takes the form,

$$R^{(N)}(\mathbf{x}, j\Delta z) = \sum_{n=1}^{N} \left[R^{(n)}(\mathbf{x}, j\Delta z) + \sum_{n' \neq n}^{N} R^{(n,n')}(\mathbf{x}, j\Delta z) \right]. \tag{8}$$

In this expression, each partial reflection coefficient $R^{(n)}$ (equation (6)) provides the correct contribution relative to the nth shot-gather. Any other term, $R^{(n,n')}$, is a spurious correction representing, in the $(\mathbf{x}, t)$-domain, the zero-lag time correlation between the wavefield emitted by the nth source and the depth extrapolated wavefield relative to the n'th shot-gather,

and given by

$$R^{(n,n')}(\mathbf{x},\, j\Delta z) = \sum_{\omega} \hat{p}_{\mathrm{s}}^{(n)}\,(\mathbf{x},\, j\Delta z, \omega)\, \hat{p}_{\mathrm{g}}^{(n')}\,(\mathbf{x},\, j\Delta z, \omega)\,. \qquad (9)$$

In fact, when the distance $||\mathbf{s}_n - \mathbf{s}_{n'}||$ between two sources, n and n', is large enough, a poor temporal coincidence between $p_{\mathrm{s}}^{(n)}$ and $p_{\mathrm{g}}^{(n')}$ is expected at each reflector position, so that, in this limit, $R^{(n,n')}$ must tend pointwise to zero.

The control of all spurious terms $R^{(n,n')}$ can be formulated in different ways as a set-partitioning problem. Each set represents a cluster of S shots ($S \ll N$), where each pair of shots would have to be selected with source positions as far apart as possible. Recalling that N might be of the order of hundreds of thousands, the intractability of this optimization problem has led us to a different approach based on a Monte-Carlo estimate of (8).

MONTE-CARLO WAVEFIELD IMAGING

Since we want to make the computing cost of the processing of a very large data set affordable, we address the problem of imaging the subsurface by implementing a sequence of M data migrations that is as short as possible. For this purpose, M must be a small fraction of N, the total number of shots.

Our idea, which formalizes and generalizes that described by Morton and Ober (1998) and Romero *et al.* (2000), is to construct a new prestack section, multiplying each Fourier component ω of the nth source wavelet by a complex number $a_{n,\omega}$ and each Fourier component of the associated recorded wavefields by its complex conjugate $a^*_{n,\omega}$. Observe that each multiplication implies a *phase* shift of both emitted and received signals and, depending on the modulus of $a_{n,\omega}$, also a change of *amplitude*. A unique source term and a unique shot-gather are then assembled in the space–frequency domain by superposing all modified source wavelets and seismic traces. The resulting prestacked volume,

$$\hat{Q}^{(N)}(\mathbf{x}_{\mathrm{s}}, \mathbf{x}_{\mathrm{g}}, \omega) = \sum_{n=1}^{N} a_{n,\omega}\, \delta(\mathbf{x}_{\mathrm{s}} - \mathbf{s}_n) \sum_{n'=1}^{N} a^*_{n',\omega}\, \hat{Tr}^{(n')}(\mathbf{x}_{\mathrm{g}}, \omega), \qquad (10)$$

is the initial condition for the depth extrapolation process. The linearity of the one-way propagation (equation (3)), leads to the imaging condition, written here in terms of $\hat{p}_{\mathrm{s}}^{(n)}$ and $\hat{p}_{\mathrm{g}}^{(n)}$,

$$r^{(N)}(\mathbf{x},\, j\Delta z) = \sum_{n=1}^{N} \left[r^{(n)}(\mathbf{x},\, j\Delta z) + \sum_{n' \neq n}^{N} r^{(n,n')}(\mathbf{x},\, j\Delta z) \right], \qquad (11)$$

with

$$r^{(n)}(\mathbf{x},\, j\Delta z) = \sum_{\omega} |a_{n,\omega}|^2\, \hat{p}_{\mathrm{s}}^{(n)}\,(\mathbf{x},\, j\Delta z, \omega)\, \hat{p}_{\mathrm{g}}^{(n)}\,(\mathbf{x},\, j\Delta z, \omega)\,, \qquad (12)$$

$$r^{(n,n')}(\mathbf{x},\, j\Delta z) = \sum_{\omega} a_{n,\omega}\, a^*_{n',\omega}\, \hat{p}_{\mathrm{s}}^{(n)}\,(\mathbf{x},\, j\Delta z, \omega)\, \hat{p}_{\mathrm{g}}^{(n')}\,(\mathbf{x},\, j\Delta z, \omega)\,. \qquad (13)$$

Suppose now that the collection $a_{n,\omega}$ forms a suite of *independent*, *identically distributed*, *random variables*, then the stochastic mean values of both $r^{(n)}$ and $r^{(n,n')}$ take the form,

$$\langle\, r^{(n)}\,\rangle(\mathbf{x},\, j\Delta z) = \langle\, |\, a\, |^2\,\rangle \sum_{\omega}\, \hat{p}_{\mathrm{s}}^{(n)}\,(\mathbf{x},\, j\Delta z, \omega)\, \hat{p}_{\mathrm{g}}^{(n)}\,(\mathbf{x},\, j\Delta z, \omega)\,, \qquad (14)$$

$$\langle\, r^{(n,n')}\,\rangle(\mathbf{x},\, j\Delta z) = |\,\langle\, a\,\rangle\,|^2 \sum_{\omega}\, \hat{p}_{\mathrm{s}}^{(n)}\,(\mathbf{x},\, j\Delta z, \omega)\, \hat{p}_{\mathrm{g}}^{(n')}\,(\mathbf{x},\, j\Delta z, \omega)\,, \qquad (15)$$

where $\langle\, |\, a\,|^2\,\rangle$ denotes the mean value of the squared modulus of the random variable a, and $|\,\langle\, a\,\rangle\,|^2$ denotes the squared modulus of the mean value.

Let us assume that each random variable $a_{n,\omega}$ is independently drawn from a probability distribution function such that $\langle\, a\,\rangle = 0$ and $\langle\, |\, a\,|^2\,\rangle = 1$. Then, by computing the expectation of $r^{(N)}$ (equation (11)), we surprisingly obtain the desired result,

$$\langle\, r^{(N)}\,\rangle(\mathbf{x},\, j\Delta z) = \sum_{n=1}^{N} R^{(n)}(\mathbf{x},\, j\Delta z) = R(\mathbf{x},\, j\Delta z), \qquad (16)$$

which is the correct imaging condition, as given by (5) and (6).

To obtain numerical estimates of (16), a Monte-Carlo importance sampling strategy must be used (Hammersley and Handscomb 1964). More precisely, we run a sequence of M depth migrations starting each time from a new randomly compressed seismic volume (10). We then construct the sequence, $r_1, r_2, \ldots, r_M$, of images to form the arithmetic mean,

$$A_M\,(\mathbf{x},\, j\Delta z) = \frac{1}{M} \sum_{m=1}^{M} r_m\,(\mathbf{x},\, j\Delta z)\,. \qquad (17)$$

A_M is an unbiased estimator for (16). Monte-Carlo theory states that, as M increases, the variance of the arithmetic mean A_M decreases *pointwise* as M^{-1}. In other words, when the number M of migrations increases, the following pointwise limit almost certainly exists:

$$\lim_{M\to\infty} A_M = \langle\, r^{(N)}\,\rangle = R(\mathbf{x},\, j\Delta z). \qquad (18)$$

Limit (18) implies that the stochastic approach just described produces an image emerging from the incoherent noise of the background.

Computer experiments confirm that this form of imaging is robust in the sense that it provides a depth-migrated section that can be correctly interpreted even after a reduced number of migrations (many fewer than the number of shot-gathers). From this point of view, Monte-Carlo imaging of compressed seismic data might constitute a breakthrough in the processing of industrial seismic acquisitions.

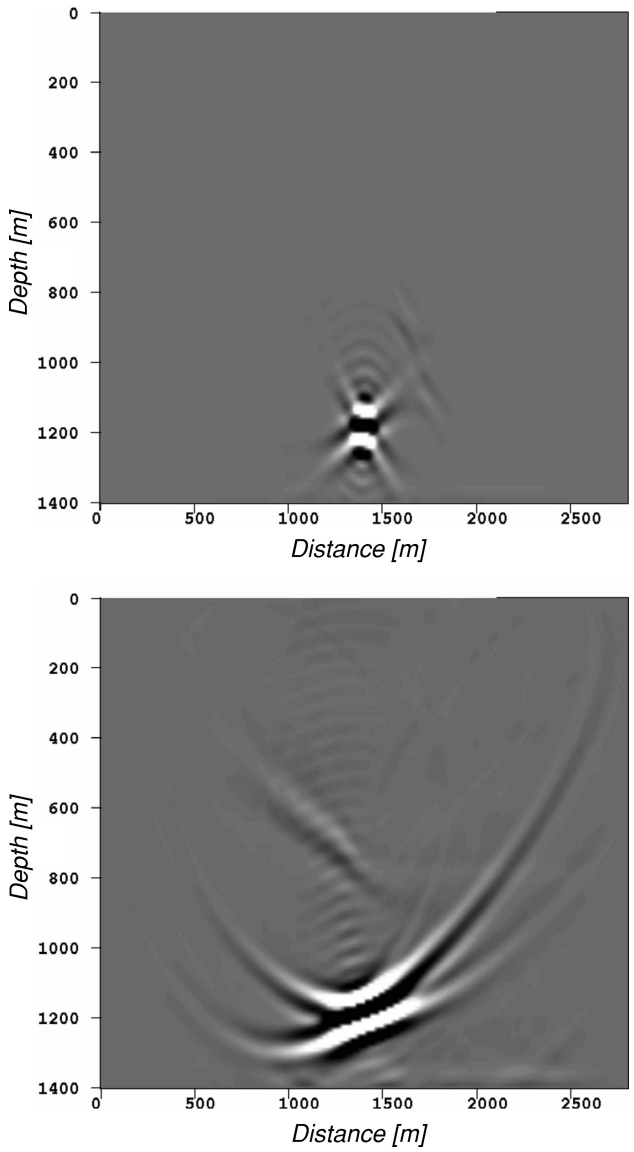

Figure 1 Scatterer images resulting from the standard shot-gather processing (top) and from the migration of one source and one shot-gather, both compressed with no encoding (bottom).

To illustrate the Monte-Carlo method, we first studied the imaging of a single point scatterer at depth 1200 m in a 2D constant velocity field of v=4000 m/s. The synthetic data set, constructed with a finite-difference solver, simulates a marine acquisition composed of 90 shot-gathers with a far offset equal to 1000 m. The migration domain is 1400 m × 3000 m, $\Delta x = \Delta z = 10$ m, the recording time is 4 s and $\Delta t = 4$ ms. Figure 1 (top) shows the scatterer image reconstructed by the standard shot-by-shot processing.

A code implementing a finite-difference extrapolation kernel operating in the frequency domain was used for an initial 2D test presented in this work. In a first computer experiment, a unique source term and a unique shot-gather of seismic traces were constructed by summing, respectively, all sources and the 90 shot-gathers with no random encoding at all. This situation corresponds to setting $a_{\omega,n} = 1$ in (10). Figure 1 (bottom) shows the resulting image: the scatterer is completely delocalized and unrecognizable.

In a second computer experiment, a sequence of migrations with randomly compressed sources and shot-gathers was run. The value +1 or −1 was assigned with probability 1/2 to each coefficient $a_{\omega,n}$ of (10). This last probability distribution satisfies both conditions $< a > = 0$ and $< a^2 > = 1$. Figure 2 (top) shows the scatterer image after only one migration: the correct structure is barely discernable through the background noise. Averaging a sequence of M images, the level of noise decreases in agreement with the analysis presented in the previous section. For this example, the noise reduction displayed in Fig. 3 demonstrates that, after about 20 Monte-Carlo steps, the relative error, namely the random noise level, has decreased by more than one order of magnitude, making the reconstructed scatterer already clearly interpretable as shown in Fig. 2 (bottom).

The same study was performed twice more: once by randomly encoding the phase of each source and shot-gather, $a_{\omega,n} = \exp(\mathrm{i}\theta_{\omega,n})$ with $\theta_{\omega,n}$ uniformly distributed inside the interval $(0, 2\pi)$, as implemented by Morton and Ober (1998). Observe that even in this case we have $< a > = 0$ and $<|a|^2> = 1$. Another possibility that was tested consists of sampling $a_{\omega,n}$ in a Gaussian probability distribution function with mean 0 and variance 1. In other words, this last encoding multiplies every Fourier component of the signal by a different real number (in the range between $\pm\infty$), thus leaving the phases of the spectrum untouched, apart from a sign.

The results of these tests are summarized in Fig. 3, which illustrates the behaviour in M^{-1} of the squared L_2-norm measuring the difference between the 'real' image (standard shot-by-shot processing) and the average image defined by (17). Observe that the three implemented sampling methods provide statistically similar images for any value of M and that the correct reconstruction is *also* possible by adequately changing only the amplitude of the extrapolated signals. In this figure, we extrapolated to $M = 100$ in order to demonstrate the validity of our theory, although from a practical point of view, this is a non-sense since in this example we deal with only 90 shots.

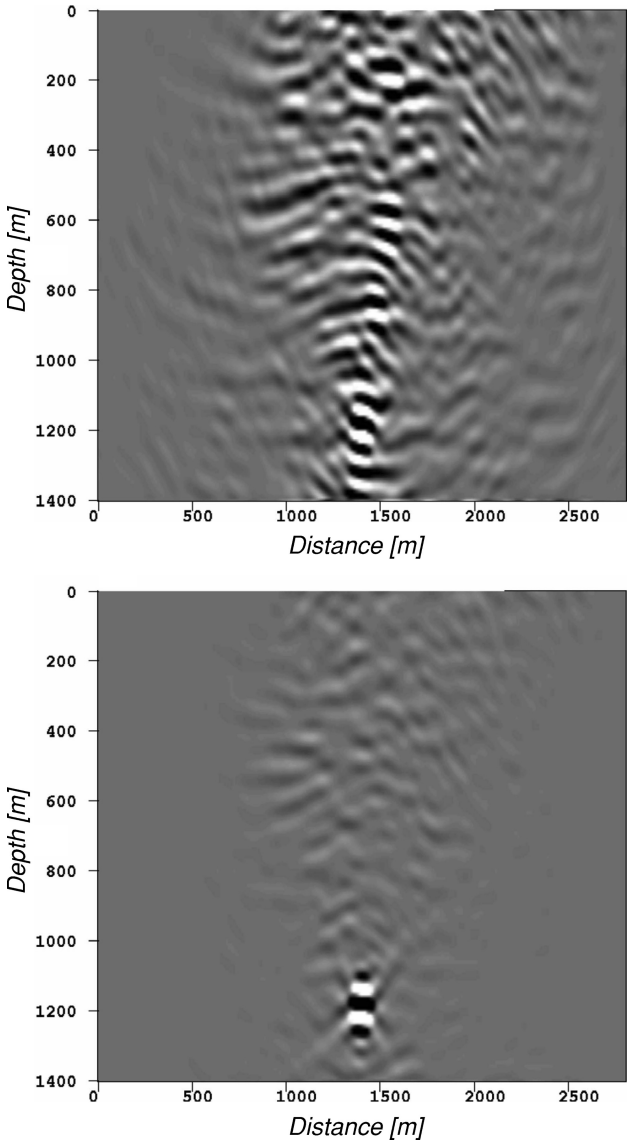

Figure 2 Scatterer images obtained from the depth extrapolation of one source and one shot-gather, both compressed implementing equation (10) with $\pm$ 1 random encoding: result after one migration (top) and result after 20 Monte-Carlo migrations (bottom).

3D IMPLEMENTATION AND EXAMPLES

From equation (B5), which describes the prestack downward extrapolation, we have concluded that, as long as seismic data are represented in the field coordinate system, source and receiver can be independently extrapolated. Whereas depth extrapolation in a stratified medium can be handled piecewise with the simple phase-shift formula, the case with lateral velocity variations requires more attention.

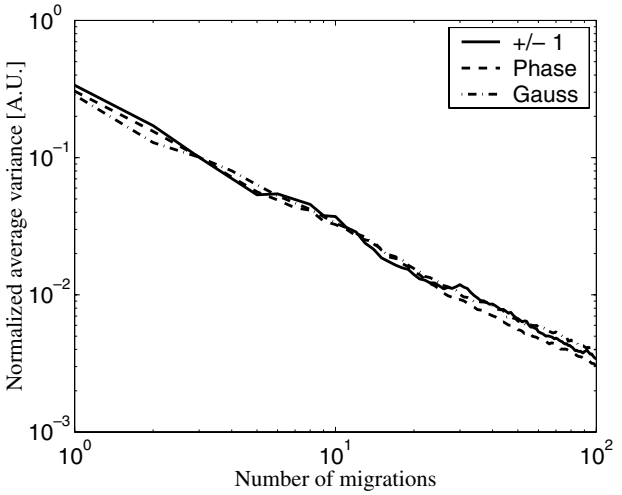

Figure 3 The drastic noise reduction shown in Fig. 2 is illustrated by the behaviour of the squared L_2-norm of the relative error, inversely proportional to the number of partial migrations. As expected, the three sampling methods, i.e. the random phase encoding, the $\pm$ 1 distribution and the Gaussian law, are statistically equivalent.

To overcome this difficulty and still keep the computational complexity of the migration to a minimum, the phase-shift plus interpolation (PSPI) method proposed by Gazdag and Sguazzero (1984) provides an extrapolation kernel in which the wave propagation is modified in order to obtain a pure spectral method for downward extrapolation in an inhomogeneous medium. Its computational advantage is that each reference solution required by the PSPI algorithm is obtained from a constant-velocity extrapolation whose implementation inherits the parallel structure of the phase-shift algorithm. Reference velocities play a crucial role, but optimizing their number and their choice had not been considered before our implementation, described in detail by Bonomi *et al.* (1998).

SEG–EAGE salt model

The SEG–EAGE Narrow Angle data set or C3-NA was chosen to illustrate the capabilities of our Monte-Carlo imaging formulation, implemented using the 3D PSPI extrapolator kernel described above (Cazzola *et al.* 2001). The performance of the resulting overall methodology was compared with the standard shot-by-shot wave migration using the same depth extrapolator. Altogether the C3-NA data set consists of about 4800 shot-gathers. We decided to migrate 10% of these shot-gathers, randomly chosen from the data set, performing 480 shot-by-shot migrations. To obtain a fair comparison between the two implementations, we ran 480 Monte-Carlo steps,

requiring exactly the same computing time as that of the decimated volume.

In order to obtain a reference image for comparison, we also migrated the entire data set shot-by-shot; the computing cost of this migrated volume is *ten times* larger than the cost of each of the other two runs and is done in this case only for purposes of comparison.

Figures 4–7 illustrate the velocity field and the migration results relative to cross-line 350 of the SEG–EAGE salt model. Figure 5 shows an image that corresponds to the shot-by-shot extrapolation of 10% of the shot-gathers; migration smiles, due to the reduced surface coverage resulting from the shot decimation, are clearly present here, especially on the first two kilometres of the depth section.

Figure 6 shows the Monte-Carlo imaging of the same cross-line after 480 steps. In this test, PSPI and the Monte-Carlo imaging provide an image very close to the one obtained by sequentially migrating all shot-gathers (Fig. 7). The migration smiles that plague the shot-by-shot approach on a decimated input cannot be present with the Monte-Carlo method, since it exploits the full coverage of the data set. Even the level of random noise present in Fig. 6 is lower than that of Fig. 5. As previously mentioned, the background noise intrinsic to this stochastic imaging algorithm can be attenuated according to (18) by increasing the number of partial images.

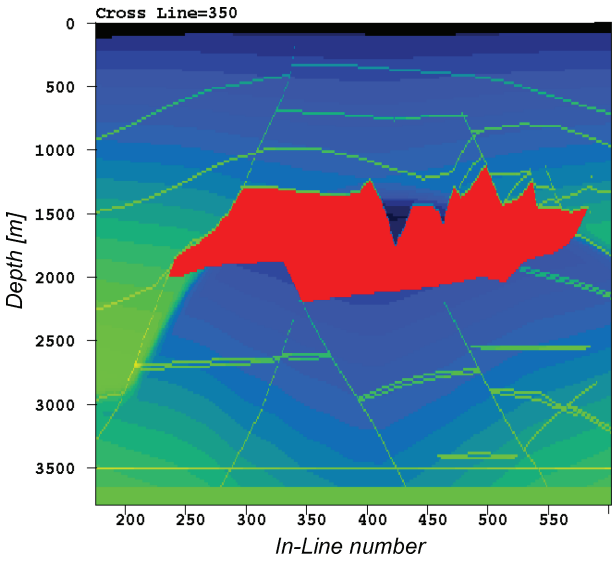

Figure 4 Cross-line 350 of the SEG–EAGE salt model: the velocity field.

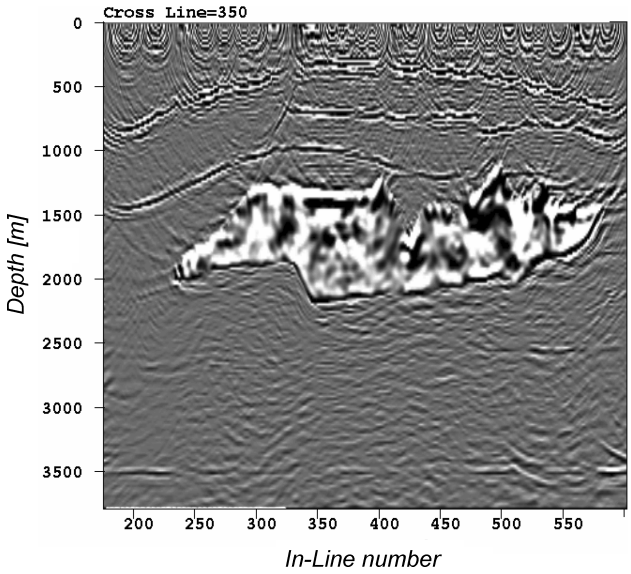

Figure 5 Cross-line 350 of the SEG–EAGE salt model: shot-by-shot migration. 480 shot-gathers, corresponding to 10% of the entire data set, were randomly selected and depth extrapolated. The migration smiles are due to the reduced surface coverage resulting from the shot decimation.

Field data

Monte-Carlo imaging with PSPI downward extrapolation has been tested on a challenging 3D data set from the Gulf of Suez, characterized by poor signal-to-noise ratio, irregular coverage and, above all, salt diapirism. Furthermore, the acquisition direction in this area was forced by operational constraints to follow the geological strike. This, in conjunction with the steep dips of the salt flanks, penalizes Kirchhoff migration, which generates strong artefacts that obscure the subsalt reflections and make the interpretation of the salt base particularly difficult (Fig. 8).

Figure 9 shows the result of Monte-Carlo migration after 1100 iterations. As the migrated area corresponds to about 22 000 shots, the computing time is reduced by a factor of approximately 18 if compared with the performance of the standard shot-by-shot wave-equation migration. Wave-equation migration permits us to delineate the salt base, indicated in Fig. 9 by the two arrows, and even to distinguish some of the weak events below. For instance, artefacts subparallel to the surface and present in the Kirchhoff reconstruction no longer appear with the wavefield approach. Even the top of the salt dome is better reconstructed. In this example, where Kirchhoff migration is inadequate to handle the complexity of the subsurface and the standard wave-equation approach

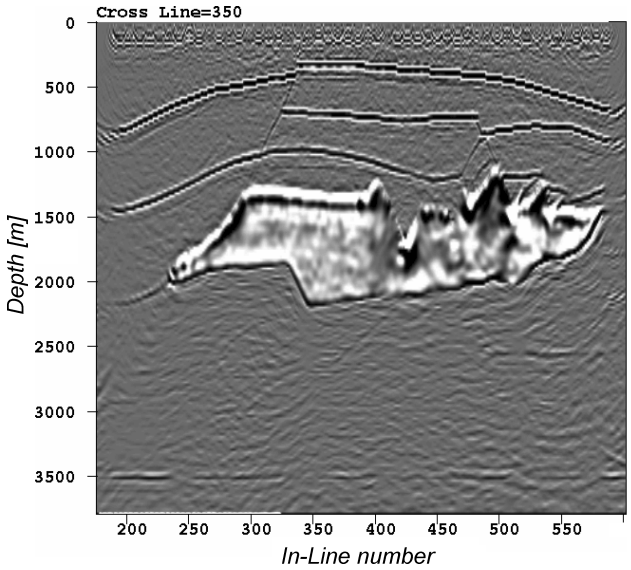

Figure 6 Cross-line 350 of the SEG–EAGE salt model: Monte-Carlo imaging. After 480 steps, PSPI and the Monte-Carlo imaging provide an image close to the one shown in Fig. 7, obtained by sequentially migrating all shot-gathers.

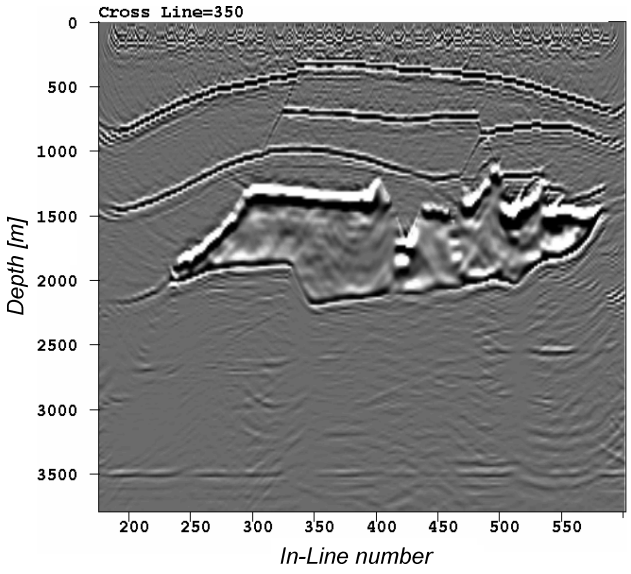

Figure 7 Cross-line 350 of the SEG–EAGE salt model: shot-by-shot migration of the entire data set.

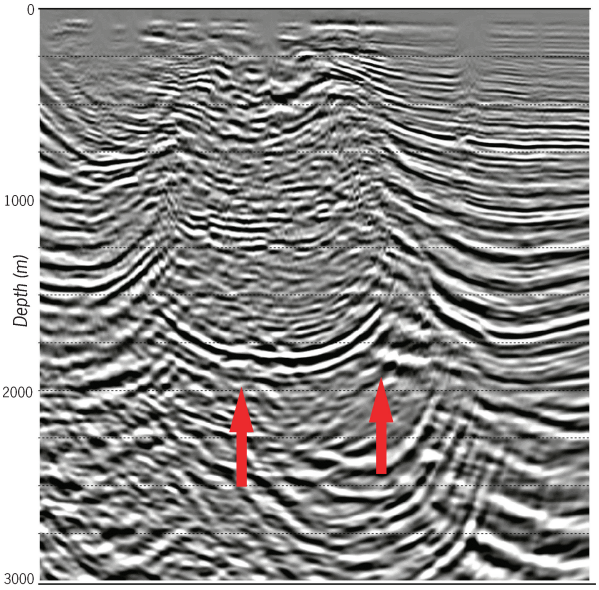

Figure 8 Gulf of Suez data set: Kirchhoff migration. Strong artefacts obscure subsalt reflections and make the interpretation of the salt base very difficult.

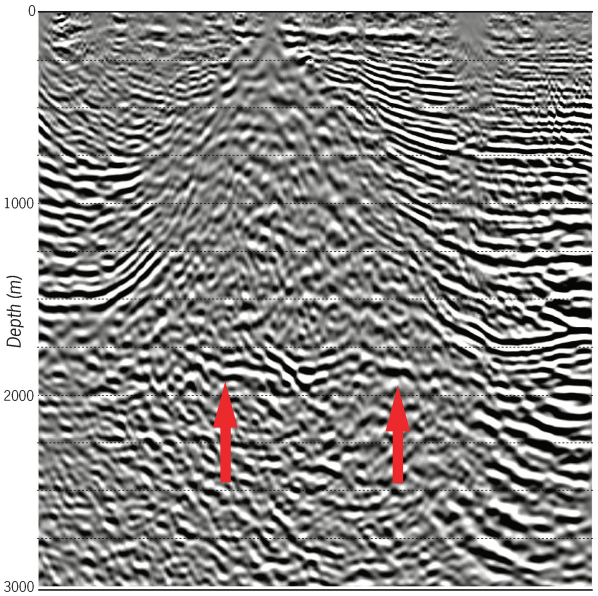

Figure 9 Gulf of Suez data set: Monte-Carlo migration after 1100 iterations. The arrows indicate the salt base. Wave-equation migration permits us to delineate the salt base and even to distinguish some of the weak events below.

appears too costly, our Monte-Carlo strategy leads to a practicable imaging solution.

CONCLUSION

The goal of this work has been to provide a theoretical framework for collectively migrating a large number of shot gathers from a single data set, using a stochastic encoding technique. With this, we are assured that by running a sequence of migrations with randomly encoded volumes, the noise level of the average image decreases asymptotically to zero.

The Monte-Carlo imaging strategy described here was implemented with a PSPI extrapolation kernel and then tested on two complex 3D data sets: the SEG–EAGE synthetic salt model and a data set acquired in the Gulf of Suez. In these two complicated examples, the Monte-Carlo approach has demonstrated itself to be a viable cost-effective industrial solution, with results in both cases superior to those achieved using standard Kirchhoff migration.

We conclude that Monte-Carlo imaging is a migration method that has the potential to become a new standard for 3D prestack wavefield depth migration. The main advantage of the stochastic approach is that it enables shot-profile wave-equation migration to be performed at sustainable computing costs, even with large production data sets (Cazzola *et al.* 2004).

ACKNOWLEDGMENTS

The authors thank ENI E&P Division, IEOC Production and Agiba Petroleum Company for permission to publish, Patrizia Cibin and Flavio Doniselli for providing the Kirchhoff migration results and Luca Bertelli and Cristiano Salino for their encouragement. They also thank Giovanni Cardone and the referees who made many helpful suggestions that improved the presentation of the results of this paper.

REFERENCES

Bleistein N., Cohen J.K. and Stockwell J.W. 2001. *Mathematics of Multidimensional Seismic Imaging, Migration and Inversion*. Springer Verlag, Inc.

Bonomi E., Brieger L.M., Nardone C.M. and Pieroni E. 1998. PSPI: a scheme for high performance echo-reconstructive imaging. *Computers in Physics* **12**, 126–132.

Bonomi E. and Cazzola L. 1999. Prestack imaging of compressed seismic data: a Monte Carlo approach. 69th SEG Meeting, Houston, USA, Expanded Abstracts, 1914–1917.

Brieger L. 2000. HPF to OpenMP on the Origin2000: a case study. *Concurrency: Practice and Experience* **12**, 1147–1154.

Cazzola L., Bonomi E., Brieger L.M. and Zanoletti F. 2001. Monte Carlo wavefield imaging of 3D prestack data. 63rd EAGE Conference, Amsterdam, The Netherlands, Extended Abstracts, Session A-26.

Cazzola L., Pizzaferri L., Ratti L., Cardone G. and Bonomi E. 2004. An example of wavefield depth migration and Monte Carlo imaging in West Africa deep waters. 74th SEG Meeting, Denver, USA, Expanded Abstracts, 1037–1040.

Collino F. and Joly P. 1995. Splitting operators, alternate directions, and paraxial approximations for the three-dimensional wave equation. *SIAM Journal on Scientific Computing* **16**, 1019–1048.

Ehinger A., Lailly P. and Marfurt K.J. 1996. Green's function implementation of common-offset, wave-equation migration. *Geophysics* **61**, 1813–1821.

Gazdag J. 1978. Wave equation migration with the phase shift method. *Geophysics* **43**, 1342–1351.

Gazdag J. and Sguazzero P. 1984. Migration of seismic data by phase-shift plus interpolation. *Geophysics* **49**, 124–131.

Gray S.H., Etgen J., Dellinger J. and Whitmore D. 2001. Seismic migration problems and solutions. *Geophysics* **66**, 1622–1640.

Hale D. 1991. 3-D depth migration by McClellan transformations. *Geophysics* **56**, 1778–1785.

Hammersley J.M. and Handscomb D.C. 1964 *Monte Carlo Methods*. Chapman and Hall, London.

Hill N.R. 2001. Prestack Gaussian-beam depth migration. *Geophysics* **66**, 1240–1250.

Morton S.A. and Ober C.C. 1998. Faster shot-record depth migrations using phase encoding. 68th SEG Meeting, New Orleans, USA, Expanded Abstracts, 1131–1134.

Notfors C., Gray S.H. and Bleistein N. 2003. Imaging using multi-arrivals: Gaussian beams or multi-arrival Kirchhoff. 65th EAGE Conference, Stavanger, Norway, Extended Abstracts, E03.

Ober C.C., Oldfield R.A., Womble D.E. and Mosher C.C. 1997. Seismic imaging on massively parallel computers. 67th SEG Meeting, Dallas, USA, Expanded Abstracts, 1418–1421.

Romero L.A., Ghiglia D.C., Ober C.C. and Morton S.A. 2000. Phase encoding of shots records in prestack migration. *Geophysics* **65**, 426–436.

Stolt R.H. 1978. Migration by Fourier transform. *Geophysics* **43**, 23–48.

Stolt R.H. and Benson A.K. 1986. *Seismic Migration*, Volume 5. Geophysical Press, London.

Xu S., Chauris H. and Noble M. 2001. Common-angle migration: a strategy for imaging complex media. *Geophysics* **66**, 1877–1894.

Yilmaz Ö. 1987. *Seismic Data Processing*. Investigation in Geophysics 2. Society of Exploration Geophysicists.

APPENDIX A

Depth wavefield extrapolation formula

In this appendix, we derive the depth extrapolation formula (equation (3)), which is valid for prestacked seismic data gathered in the shot–receiver domain. To begin we assume that the wave velocity c is constant. Let $P(\mathbf{x}_s, z_s, \mathbf{x}_g, z_g, t)$ be represented by a Fourier series:

$$P\left(\mathbf{x}_s, z_s, \mathbf{x}_g, z_g, t\right) = \sum_{\mathbf{k}_s, \mathbf{k}_g} \sum_{\omega} \hat{P}(\mathbf{k}_s, z_s, \mathbf{k}_g, z_g, \omega) \times \exp[\mathrm{i}(\mathbf{k}_s \cdot \mathbf{x}_s + \mathbf{k}_g \cdot \mathbf{x}_g + \omega t)], \quad \text{(A1)}$$

where $\mathbf{k}_s, \mathbf{k}_g$ are respectively the source and receiver wavenumber vectors and ω is the time angular frequency. Since we are interested in the depth extrapolation of the prestacked seismic volume (equation (1)), we look for the solution describing a wavefield propagating downwards. Such a solution is

$$\hat{P}\left(\mathbf{k}_s, z_s, \mathbf{k}_g, z_g, \omega\right) = \hat{Q}(\mathbf{k}_s, \mathbf{k}_g, \omega) \exp[\mathrm{i}(q_g z_g + q_s z_s)], \quad \text{(A2)}$$

$$q_g = \frac{\omega}{c}\sqrt{1 - \|\mathbf{k}_g\|^2 \left(\frac{c}{\omega}\right)^2},$$
$$q_s = \frac{\omega}{c}\sqrt{1 - \|k_s\|^2 \left(\frac{c}{\omega}\right)^2},$$

where

$$\hat{Q}(\mathbf{k}_s, \mathbf{k}_g, \omega) = \sum_{\mathbf{x}_s, \mathbf{x}_g} \sum_t Q(\mathbf{x}_s, \mathbf{x}_g, t) \times \exp[-i(\mathbf{k}_s \cdot \mathbf{x}_s + \mathbf{k}_g \cdot \mathbf{x}_g + \omega t)] \quad \text{(A3)}$$

is the Fourier-transformed prestacked volume (Stolt 1978). By imposing the condition $z_g = z_s = z$ in (A2) and setting $\hat{p}(\mathbf{k}_s, \mathbf{k}_g, z, \omega) = \hat{P}(\mathbf{k}_s, z, \mathbf{k}_g, z, \omega)$, we obtain the phase shift formula which predicts $\hat{p}$ as a result of moving both source and receiver from depth z to $z + \Delta z$ and with the prestacked volume imposed as the initial condition for the depth extrapolation, i.e. $\hat{p}(\mathbf{x}_s, \mathbf{x}_g, 0, \omega) = \hat{Q}(\mathbf{x}_s, \mathbf{x}_g, \omega)$:

$$\hat{p}\left(\mathbf{x}_s, \mathbf{x}_g, z + \Delta z, \omega\right) = \sum_{\mathbf{k}_s, \mathbf{k}_g} \hat{p}\left(\mathbf{k}_s, \mathbf{k}_g, z, \omega\right) \times \hat{W}_{\Delta z}\left(\mathbf{k}_s, \frac{\omega}{c_s}\right) \hat{W}_{\Delta z}\left(\mathbf{k}_g, \frac{\omega}{c_g}\right) \times \exp[-i(\mathbf{k}_s \cdot \mathbf{x}_s + \mathbf{k}_g \cdot \mathbf{x}_g)]. \quad \text{(A4)}$$

$\hat{W}_{\Delta z}(\mathbf{k}, \frac{\omega}{c})$ denotes the exponential downward extrapolator whose domain of application is restricted to the non-evanescent region of the Fourier domain (Gazdag 1978).

We would like to migrate data using an arbitrary velocity model; however, it is clear from the construction of (A4) that this expression is no longer valid for a velocity field $c = c(\mathbf{r})$ with lateral variations. To overcome this difficulty, it is preferable to simplify the migration model a step further, keeping its computational complexity to a reasonable level. The basic strategy adopted is the following. We start from the phase shift formula (A4), written in the space–frequency domain as a double convolution

$$\hat{p}\left(\mathbf{x}_s, \mathbf{x}_g, z + \Delta z, \omega\right) = \sum_{\mathbf{x}'_s, \mathbf{x}'_g} W_{\Delta z}\left(\mathbf{x}_s - \mathbf{x}'_s, \frac{\omega}{c_s}\right) \times W_{\Delta z}\left(\mathbf{x}_g - \mathbf{x}'_g, \frac{\omega}{c_g}\right) \times \hat{p}\left(\mathbf{x}'_s, \mathbf{x}'_g, z, \omega\right), \quad \text{(A5)}$$

where $\hat{p}(\mathbf{x}_s, \mathbf{x}_g, 0, \omega) = \hat{Q}(\mathbf{x}_s, \mathbf{x}_g, \omega)$. Finally, the imaging condition (equation (2)) yields the map of the local reflectivity displaying an acoustic image of the earth's crust:

$$R(\mathbf{x}, z + \Delta z) = \sum_{\omega} \hat{p}\left(\mathbf{x}, \mathbf{x}, z + \Delta z, \omega\right). \quad \text{(A6)}$$

The direct introduction of the velocities $c_s = c_z(\mathbf{x}'_s)$ and $c_g = c_z(\mathbf{x}'_g)$ into the extrapolating equation (A5) is not formally justifiable; however, it provides a prestack migration model for inhomogeneous media which has proved to be a very accurate imaging tool (Gray *et al.* 2001).

APPENDIX B

The one-shot problem

In this appendix, we derive equation (6), the imaging condition for a single shot gather. We assume that the prestacked seismic volume $Q(\mathbf{x}_s, \mathbf{x}_g, t)$ contains the information resulting from one shot emitted at position $\mathbf{r}_s = (\mathbf{s}, 0)$ at the surface. Thus the prestacked volume (equation (1)) takes the form,

$$Q(\mathbf{x}_s, \mathbf{x}_g, t) = \delta(\mathbf{x}_s - \mathbf{s}) Tr(\mathbf{x}_g, t), \quad \text{(B1)}$$

where $Tr(\mathbf{x}_g, t)$ represents the collection of seismic traces recorded during the experiment. Introducing the initial condition (B1) into (A5) after the first iteration step, the following extrapolated wavefield results:

$$\hat{p}\left(\mathbf{x}_s, \mathbf{x}_g, \Delta z, \omega\right) = W_{\Delta z}\left(\mathbf{x}_s - \mathbf{s}, \frac{\omega}{c_s}\right) \hat{p}_g\left(\mathbf{x}_g, \Delta z, \omega\right) = \hat{p}_s\left(\mathbf{x}_s, \Delta z, \omega\right) \hat{p}_g\left(\mathbf{x}_g, \Delta z, \omega\right). \quad \text{(B2)}$$

Note that the wavefield $\hat{p}_s(\mathbf{x}_s, \Delta z, \omega)$ is formally identical to the extrapolated wavefield produced by the purely symmetric, impulsive source,

$$p_s\left(\mathbf{x}_s, 0, t\right) = \delta(\mathbf{x}_s - \mathbf{s})\delta(t). \quad \text{(B3)}$$

The wavefield $\hat{p}_g(\mathbf{x}_g, \Delta z, \omega)$ represents the prediction on the seismic traces, assuming the receivers inside the earth are at level Δz. This prediction is determined by the surface condition,

$$p_g\left(\mathbf{x}_g, 0, t\right) = Tr(\mathbf{x}_g, t). \quad \text{(B4)}$$

Introducing both conditions (B3) and (B4) into (A5), we obtain the value of $\hat{p}$ that would be valid for source and receivers inside the earth at each depth multiple of Δz:

$$\hat{p}\left(\mathbf{x}_s, \mathbf{x}_g, j\Delta z, \omega\right) = \hat{p}_s\left(\mathbf{x}_s, j\Delta z, \omega\right) \hat{p}_g\left(\mathbf{x}_g, j\Delta z, \omega\right), \quad j = 1, 2, \ldots, \quad \text{(B5)}$$

where both fields, $\hat{p}_s$ and $\hat{p}_g$, at the jth level result from the convolution between the exponential downward extrapolator W with $\hat{p}_s$ and $\hat{p}_g$ evaluated at the $(j-1)$th level. Observe that source and receiver are independently extrapolated; the only coupling between $\hat{p}_s$ and $\hat{p}_g$ is introduced through the imaging condition (equation (A6)), from which we derive the map of the local reflectivity at depth $j\Delta z$:

$$R(\mathbf{x}, j\Delta z) = \sum_{\omega} \hat{p}_s\left(\mathbf{x}, j\Delta z, \omega\right) \hat{p}_g\left(\mathbf{x}, j\Delta z, \omega\right). \quad \text{(B6)}$$